J-9 EVALUATION OF SR-90 PEAK AQUIFER CONCENTRATION BY SOURCE

Sources of Sr-90 included in the sensitivity and RI/BRA base simulations included the: tank farm sources (18,100 Ci), OU 3-13 soil sources (918 Ci), CPP-02 abandoned french drain (33.8 Ci), CPP-3 injection well failure (8.0 Ci), and percolation ponds (0.3 Ci). In addition, 16 Ci of Sr-90 were injected directly into the aquifer in well CPP-03 as service waste. The primary sources of Sr-90 in the tank farm were associated with CPP-31 (15,900 Ci) and CPP-79 deep (874 Ci), with the remaining Sr-90 originating from the OU 3-13 soil sites and from the failed injection well. The following analysis presents the evolution of Sr-90 as it migrates through the vadose zone and into the aquifer from CPP-79, CPP-31, and all other sources. In all three cases, the source geochemical model is that presented in Section J-8.

J-9.1 Contribution From All Sources of Sr-90 Excluding CPP-31 and CPP-79 Deep

The following results are presented to analyze the contribution from the sources of Sr-90 not including CPP-31 and CPP-79 deep. These sources of Sr-90 include all of the OU 3-13 Group 3 soil sites, and all of the OU 3-14 sites except CPP-31 and CPP-79 deep. These results are a subset of the model predictions presented in Section J-8, where it was assumed that the OU 3-13 Group 3 soil sites were outside the influence of acidic releases and the K_d applied in the alluvium in the base grid was 20 mL/g.

J-9.1.1 Vadose Zone Sr-90 Simulation Results

The spatial distribution of Sr-90 in the vadose zone is presented in Figures J-9-1 through J-9-4 through the year 2293. The profiles of vertical concentration show the contribution from (a) the percolation ponds and southern OU 3-13 soil sources in southern INTEC, (b) OU 3-13 soil sources and CPP-79 shallow in northern INTEC, and (c) the influence of the failed injection well at early times deep in the vadose zone (at about 1750 m from the southern boundary). The horizontal distribution shows the extensive early contribution from the failed injection well, and an isolated contribution from CPP-37B to the northeast of the tank farm. This latter contribution is probably overestimated here as discussed in Appendix A, Section 5. In fact, the source activities for most of the OU 3-13 soil sources were probably overestimated and many of those contaminated soil sources have been the target of remedial actions. Given that the activities of Sr-90 at these sites is small compared to CPP-31 and CPP-79, these source activities were not re-evaluated, and the remedial actions are not accounted for in this RI/BRA.

Peak vadose zone concentrations from these sources are represented by the red line in Figure J-9-5. Initial high concentrations between 1968 and 1990 are a result of the failed injection well. The increase in concentration occurring around year 2000 is a result of increased flows in the Big Lost River. Increasing the flow in the Big Lost River drives higher concentrations from the 380 ft interbed into the aquifer. In this plot, the highest concentrations (4.6E6 pCi/L) in the vadose zone are predicted to occur in 1990 and are (a) between the 380 ft interbed and aquifer and (b) between land surface and the lower northern perched water.

In addition to the contribution from these sources shown in red, the RI/BRA base case which included all of the Sr-90 sources is shown in black. The largest deviation occurs after 1986. These deviations represents the combined influence of CPP-31 and CPP-79 deep. At later times, the source of the deviation is the same, but the differences between predicted concentration histories are more damped, illustrating the effect of dispersive downward transport from CPP-31 and CPP-79 deep.

The rate at which the activity leaves the vadose zone and enters the aquifer is shown in Figure J-9-6. and can be compared directly to the RI/BRA base case (shown in black). The similarity of results represented by the black and red lines prior to about year 2000 shows that the majority of the total flux simulated in the RI/BRA base case (black line) originates from sites other than CPP-31 and CPP-79 deep. The very small difference in the flux magnitude between 1980 and 2000 (difference between the red and black lines) is a reflection of the early arrival from those two large activity sources.

Figure J-9-1. Sr-90 vadose zone concentration excluding CPP-31 and CPP-79 (horizontal contours) (pCi/L) (MCL = thick red line, 10*MCL = thin red line, MCL/10 = black line).

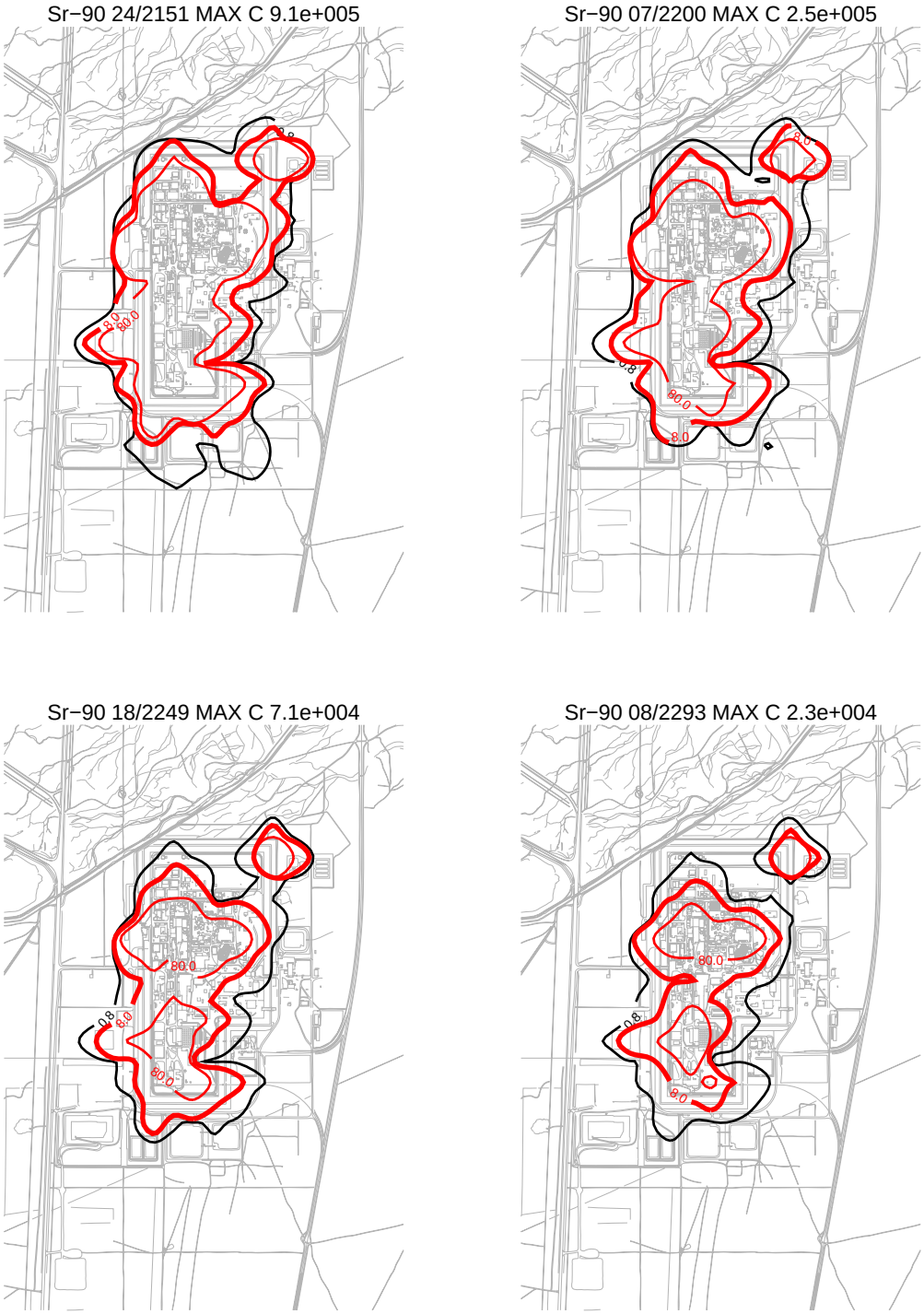

Figure J-9-2. Sr-90 vadose zone concentration excluding CPP-31 and CPP-79 (horizontal contours) (pCi/L) (MCL = thick red line, 10*MCL = thin red line, MCL/10 = black line).

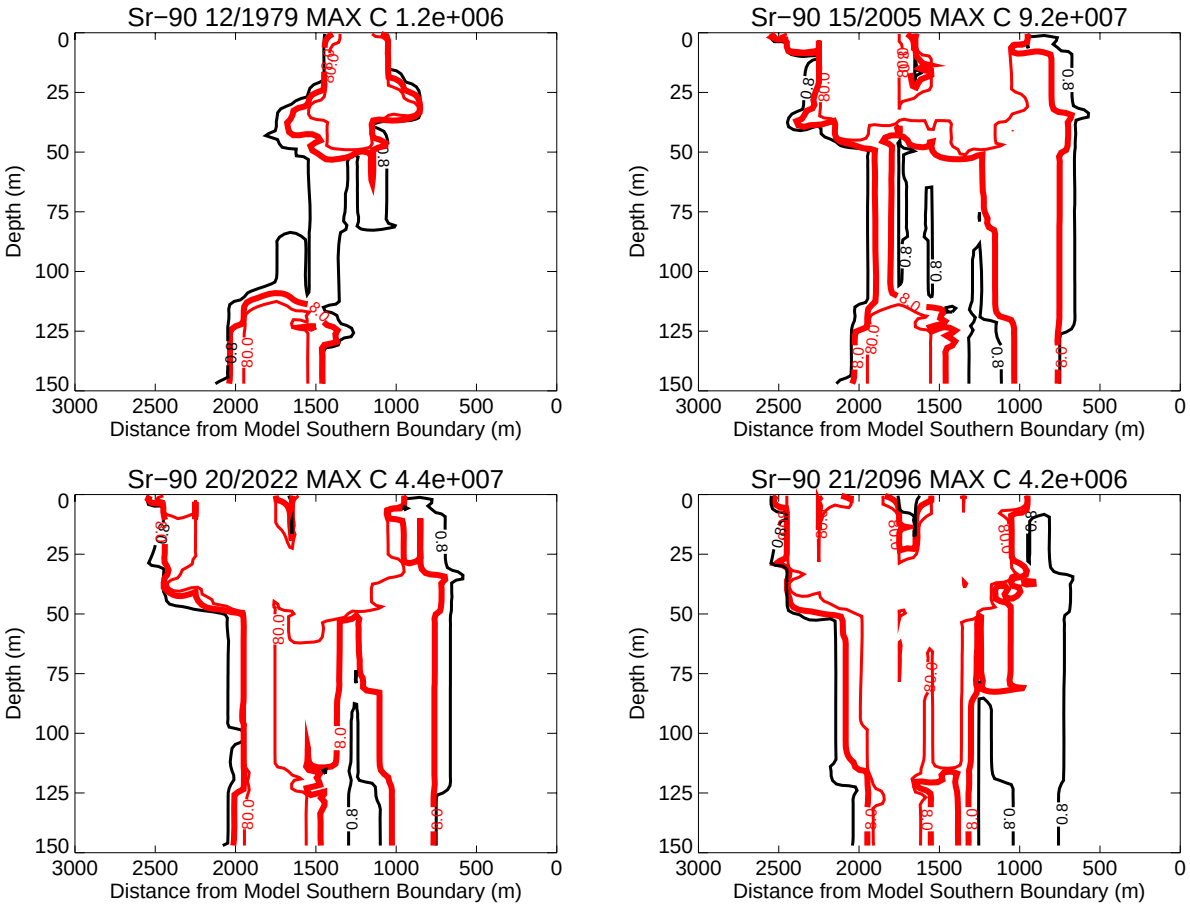

Figure J-9-3. Sr-90 vadose zone concentrations excluding CPP-31 and CPP-79 (vertical contours) (pCi/L) (MCL = thick red line, 10*MCL = thin red line, MCL/10 = black line).

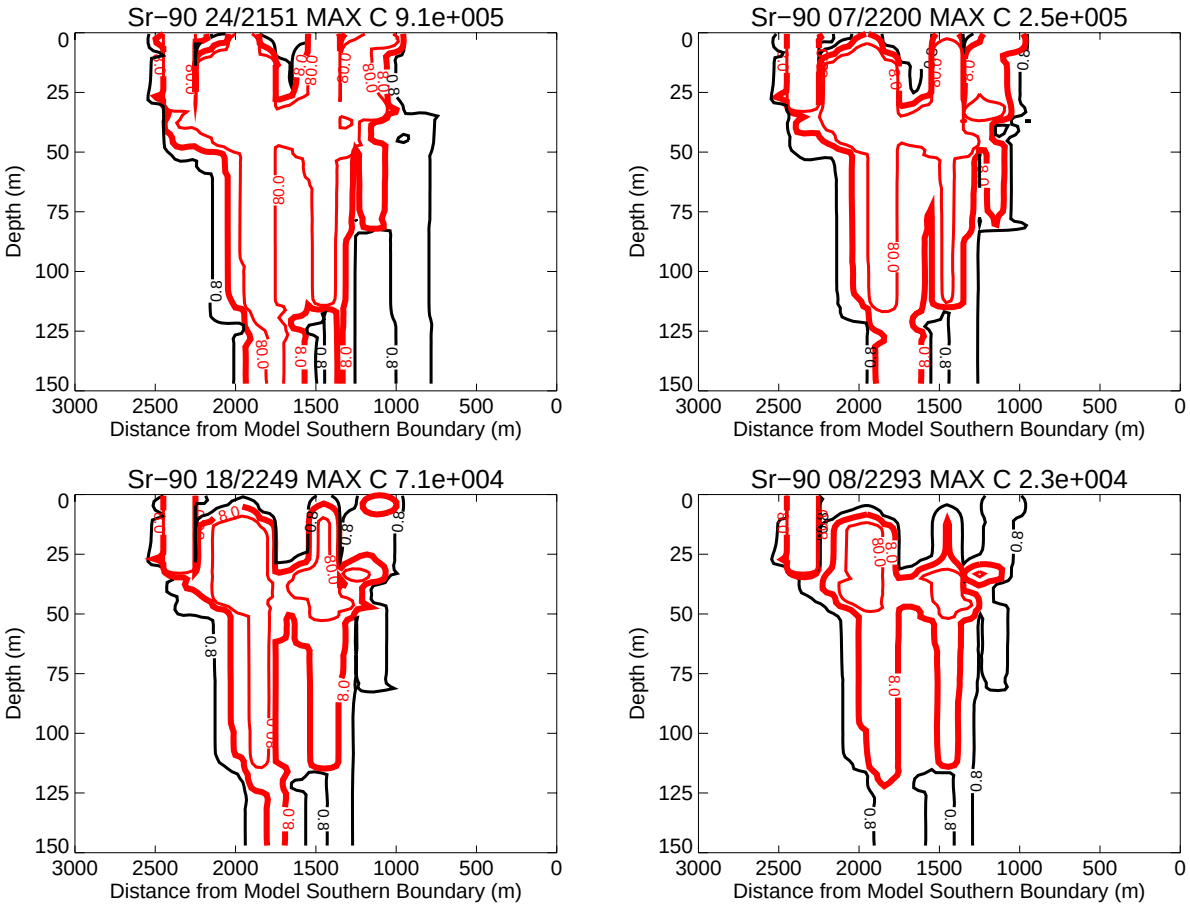

Figure J-9-4. Sr-90 vadose zone concentrations excluding CPP-31 and CPP-79 (vertical contours) (pCi/L) (continued) (MCL = thick red line, 10*MCL = thin red line, MCL/10 = black line).

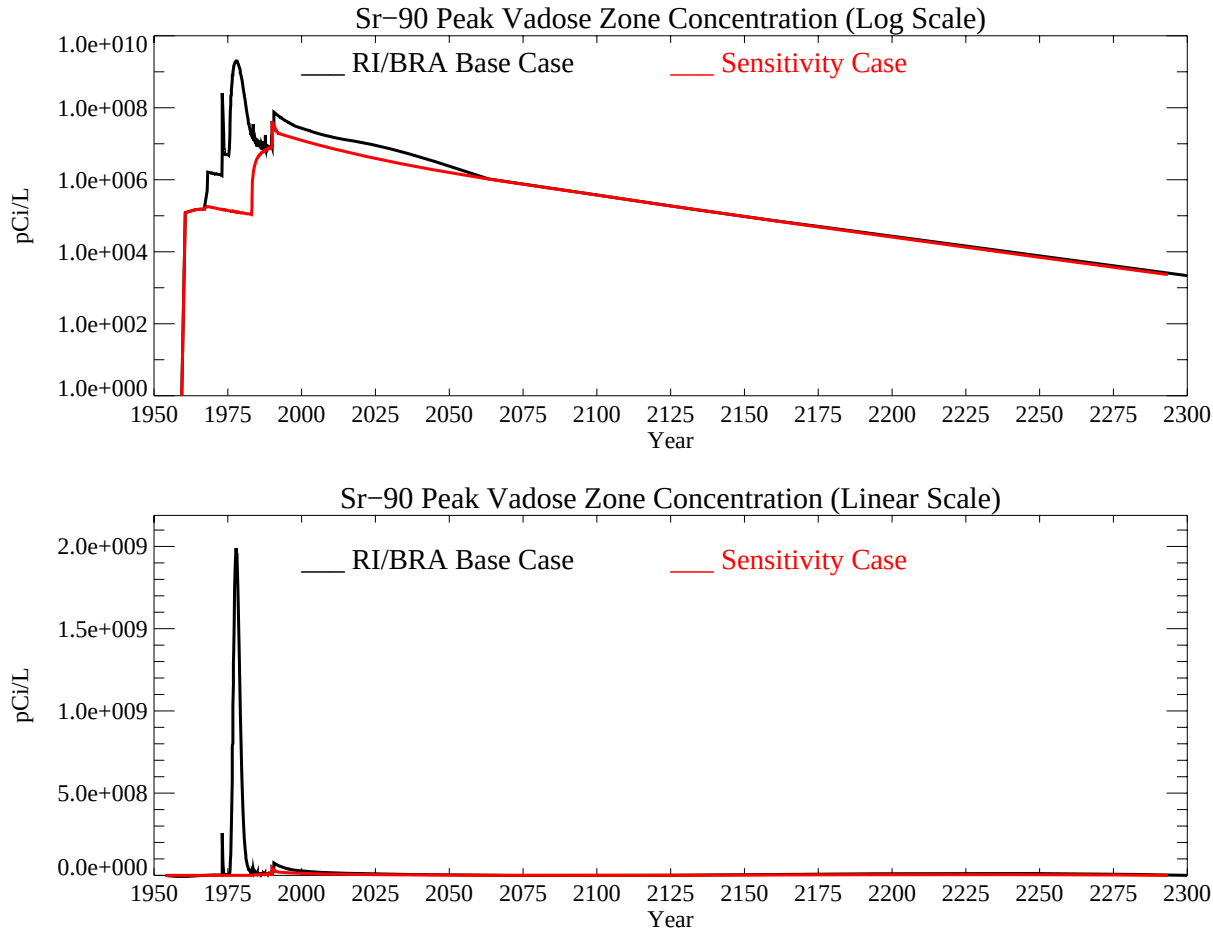

Figure J-9-5. Sr-90 peak vadose zone concentrations excluding CPP-31 and CPP-79 (pCi/L) with the RI/BRA model in black and these sources only in red.

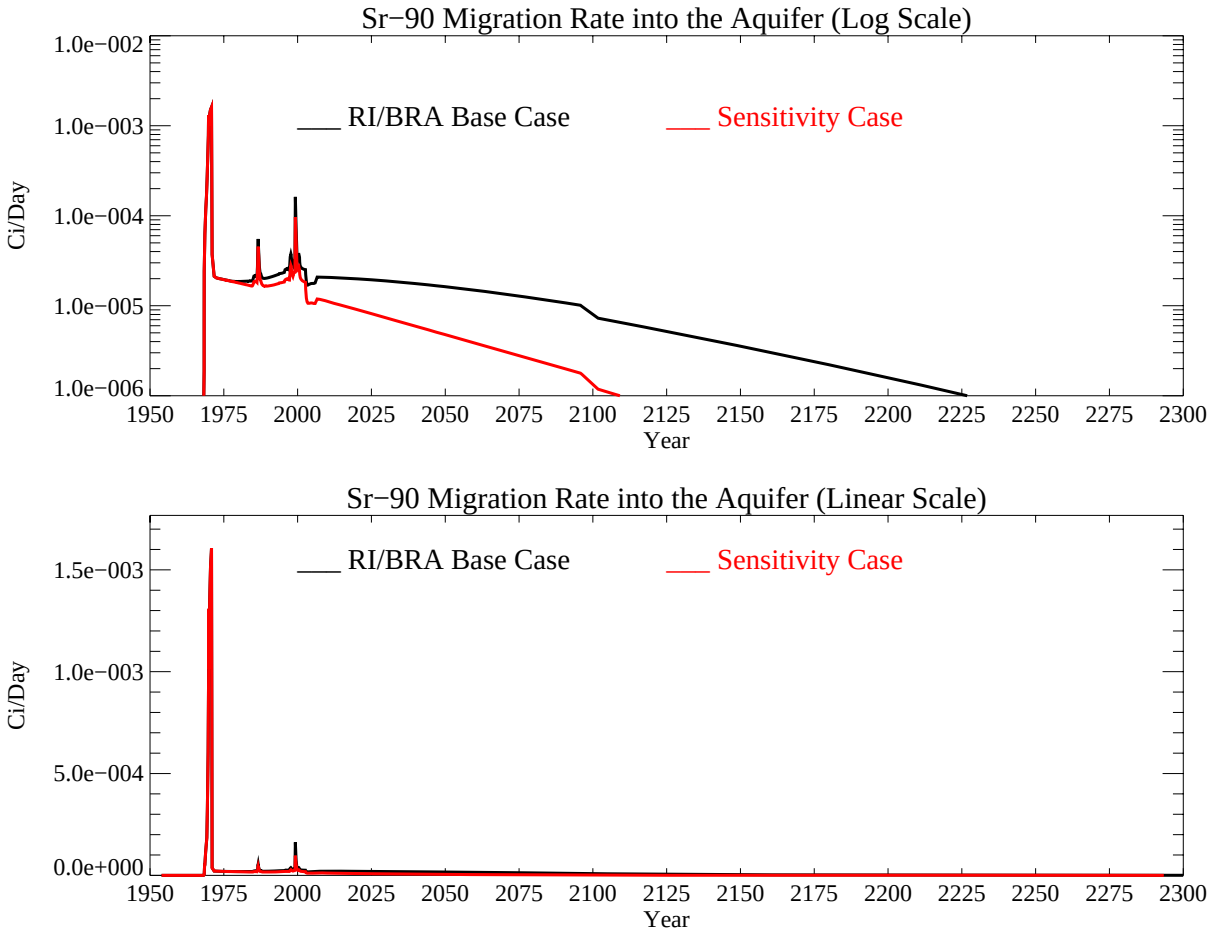

Figure J-9-6. Sr-90 activity flux into the aquifer excluding CPP-31 and CPP-79 (Ci/day) with the RI/BRA model in black, and these sources only in red.

J-9.1.2 Aquifer Sr-90 Simulation Results

The horizontal distribution of Sr-90 in the aquifer for the time period spanning 1979-2096 in the course grid is given in Figure J-9-7, and on the fine grid spanning 2096-2249 in Figure J-9-8. As with the vadose zone plots, these concentration isopleths are presented at 0.8, 8.0, and 80 pCi/L. The distribution prior to 2095 (Figure J-9-7) can be compared to that obtained considering all sources (Figure J-8-18), and shows that current aquifer concentrations primarily originate from these sources. At later times (Figures J-9-8 and J-8-19), there are significant differences illustrating the contribution from the major tank farm sources.

The resultant peak aquifer concentrations are given in Figure J-9-9. The peak aquifer Sr-90 concentration was predicted to be 5761 pCi/L in 1965 and is the result of the CPP-3 well. Simulated Sr-90 concentrations were predicted to remain above the MCL from 1960 through year 2047 from these sources and were predicted to decline after the year 2000. As shown in the RI/BRA model, there is a significant step decrease in concentration following the removal of anthropogenic water at land surface in 2095.

The predicted peak Sr-90 concentration here in the year 2095 is 3.2 pCi/L, about 17% of that predicted considering all of the sources (black line). This concentration is less than half of the MCL, underlining the importance of the vadose zone contributions. Considering these sources alone, concentrations are predicted to fall below the MCL in 2047.

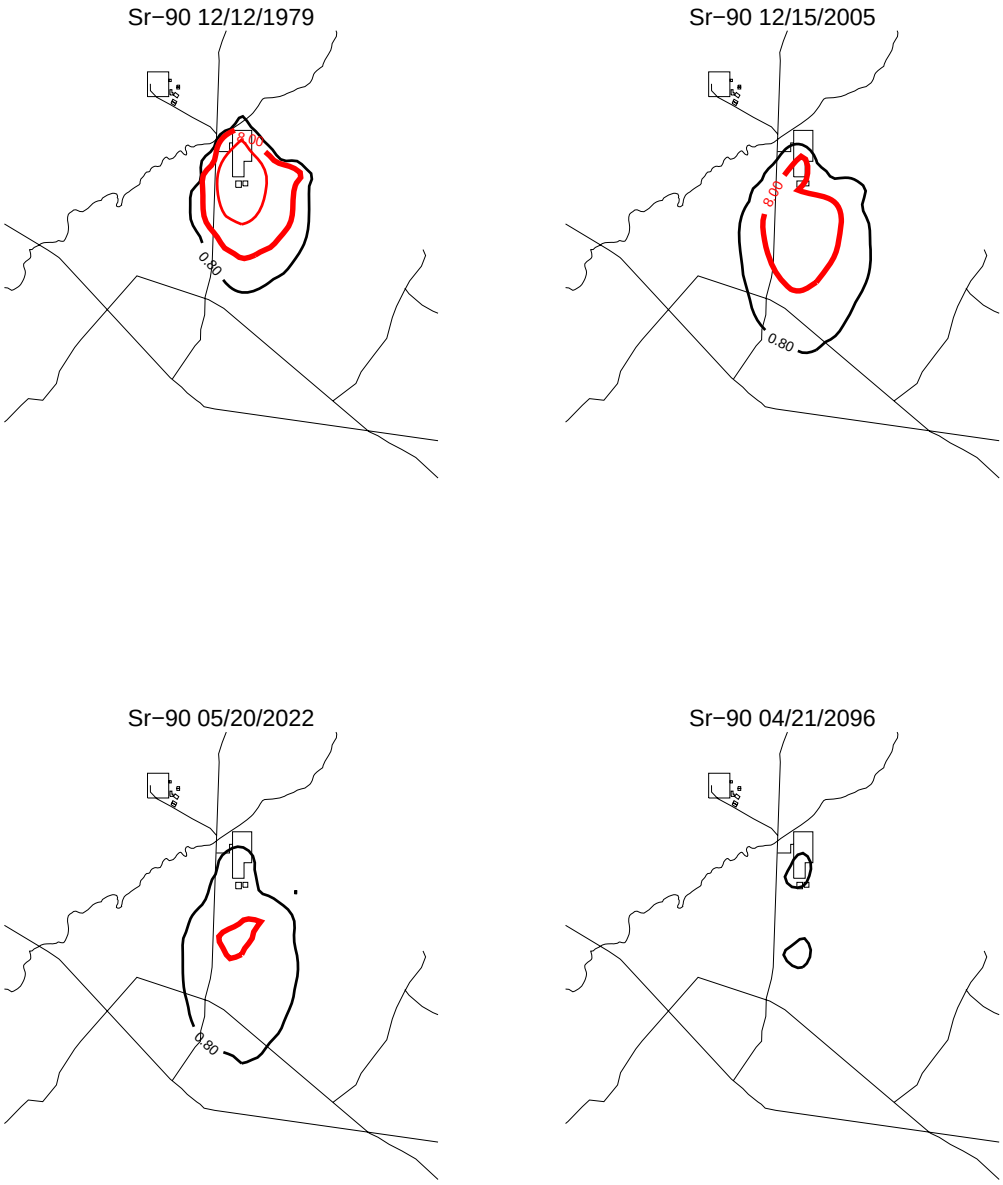

Figure J-9-7. Sr-90 aquifer concentration contours (pCi/L) (MCL = thick red line, 10*MCL = thin red line, MCL/10 = black line).

Figure J-9-8. Sr-90 aquifer concentration contours (pCi/L) (continued) (MCL = thick red line, 10*MCL = thin red line, MCL/10 = black line).

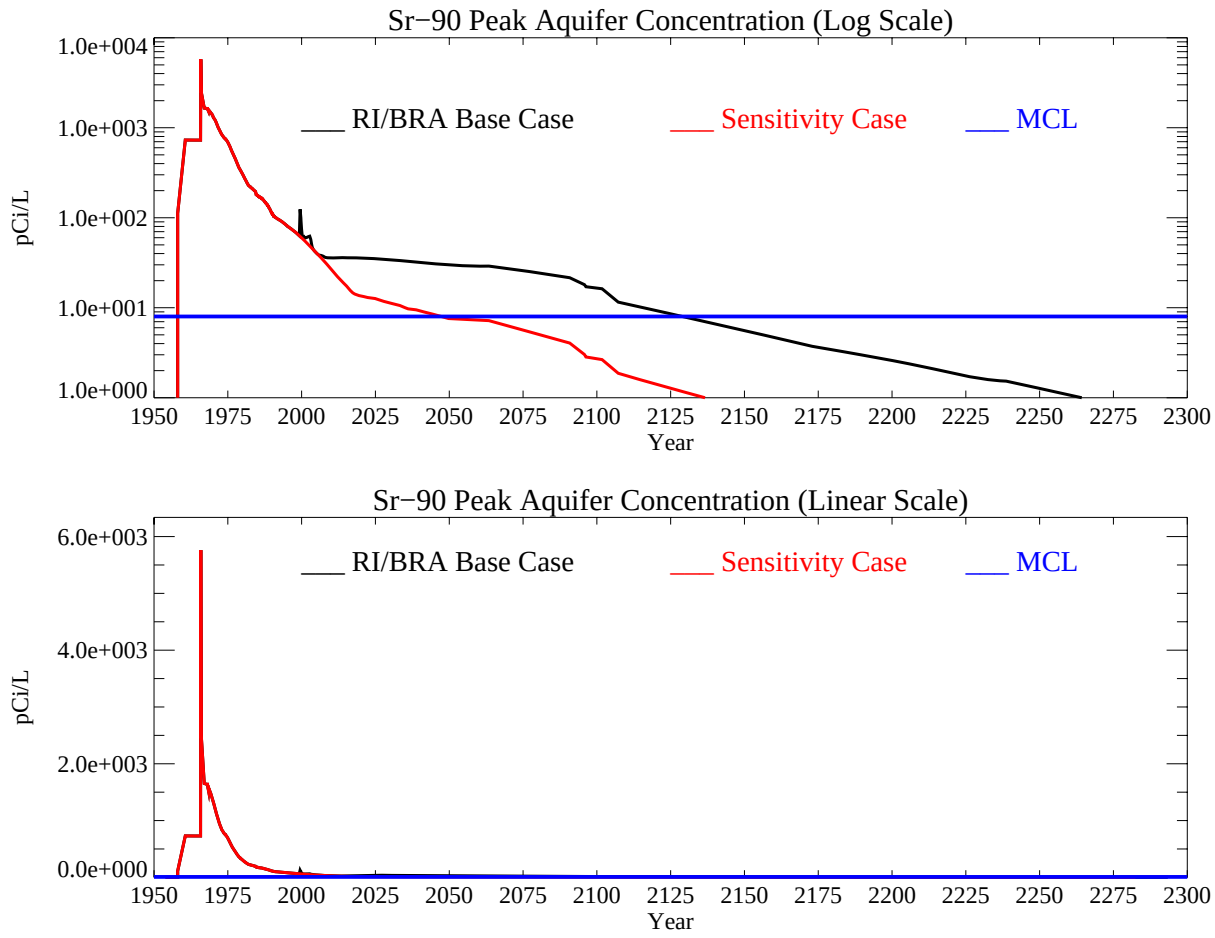

Figure J-9-9. Sr-90 peak aquifer concentrations (pCi/L) with the MCL in blue, RI/BRA model in black and these sources only in red.

J-9.2 Contribution from CPP-79 Deep

The following results are presented to analyze the contribution from just CPP-79 Deep for the RI/BRA model predictions presented in Section J-8.

J-9.2.1 Vadose Zone Sr-90 Simulation Results

The Sr-90 spatial distribution through year 2293 from CPP-79 deep is given in Figures J-9-10 through J-9-13. These can be compared to the distribution predicted for theRI/BRA base case which were presented in Figures J-8-10 through J-8-13. The vertical distribution of Sr-90 from Site CPP-79 Deep in year 1979 extends from land surface to the aquifer. This very early arrival of Sr-90 in very high pore water concentrations is a reflection of dispersive transport, and is not reflective of the advective transport that occurs at a much reduced rate. Even though the vertical profiles suggest that flow is primarily vertical, the horizontal contour plots show that the lateral extent impacted by CPP-79 in the vadose zone is extensive.

Peak vadose zone concentrations through time are given by the red line in Figure J-9-14 and are slightly below 100 pCi/L in year 2300. The step increases in concentrations are the result of the two different releases in that occurred in 1968 and again in 1973. The early arrival deep in the vadose zone is a function of (a) the CPP-79 Deep release occurring just above the basalt-alluvium interface, and (b) the vertical driving force presented by the 2500 gallon release that occurred just above CPP-79 Deep in Site CPP-79 shallow. There was actually very little water associated with CPP-79 Deep itself (only about 400 gallons). These concentrations can be compared to those obtained when all sources of Sr-90 are considered (shown in black). Although Sr-90 originating from CPP-79 deep is distributed throughout the vadose zone, the concentrations from this source are only a small percentage of the other peak concentrations. This is an artifact of the high pore water concentration that exists in the alluvium rather than an indication of whether or not CPP-79 is a major contributor to aquifer concentrations.

The rate at which the CPP-79 deep activity enters the aquifer is shown by the red line in Figure J-9-15, and can be compared directly to the RI/BRA model including all sources (shown as black). This comparison illustrates that about 10% of the activity leaving the alluvium after year 2000 originated from CPP-79 deep. This suggests that there is a significant overlapping contribution from non-CPP-31 and CPP-31during the 1990-2010 time period, and that the fluxes arriving in the aquifer after about 2010 are primarily associated with CPP-31 and CPP-79. The results showing the CPP-31 contributions are presented in Section J-9.3 and J-9.4.

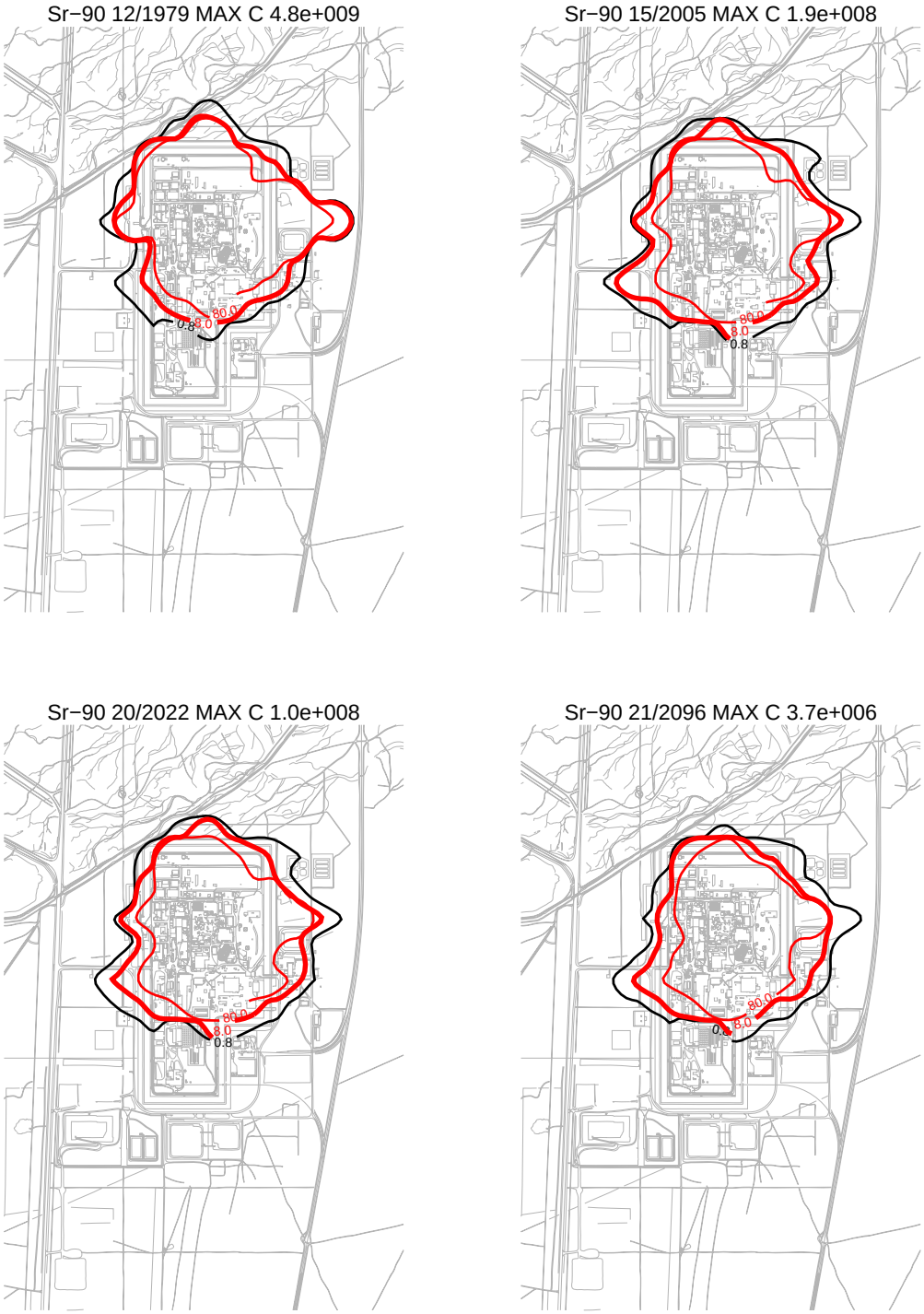

Figure J-9-10. Sr-90 vadose zone concentration from CPP-79 deep (horizontal contours) (pCi/L) (MCL = thick red line, 10*MCL = thin red line, MCL/10 = black line).

Figure J-9-11. Sr-90 vadose zone concentration from CPP-79 deep (horizontal contours) (pCi/L) (MCL = thick red line, 10*MCL = thin red line, MCL/10 = black line).

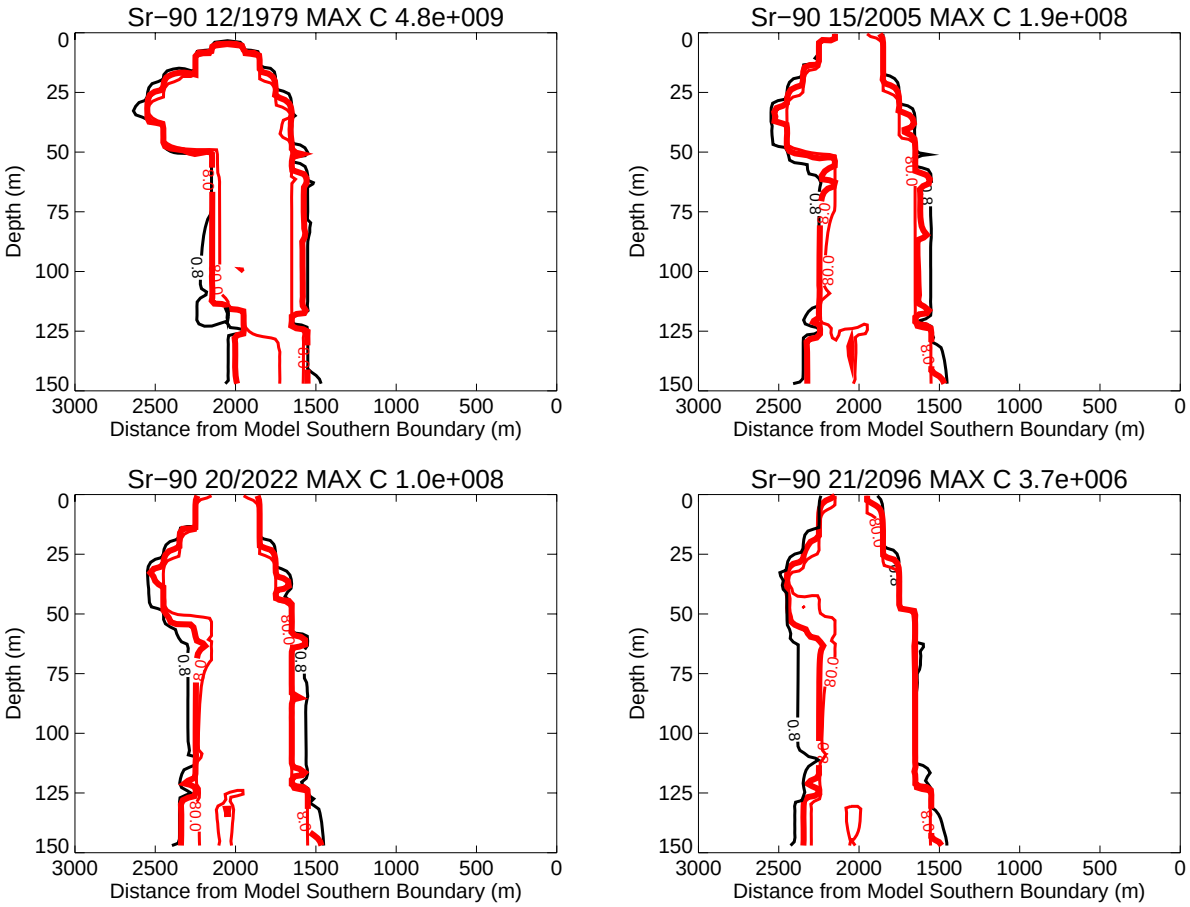

Figure J-9-12. Sr-90 vadose zone concentrations from CPP-79 deep (vertical contours) (pCi/L) (MCL = thick red line, 10*MCL = thin red line, MCL/10 = black line).

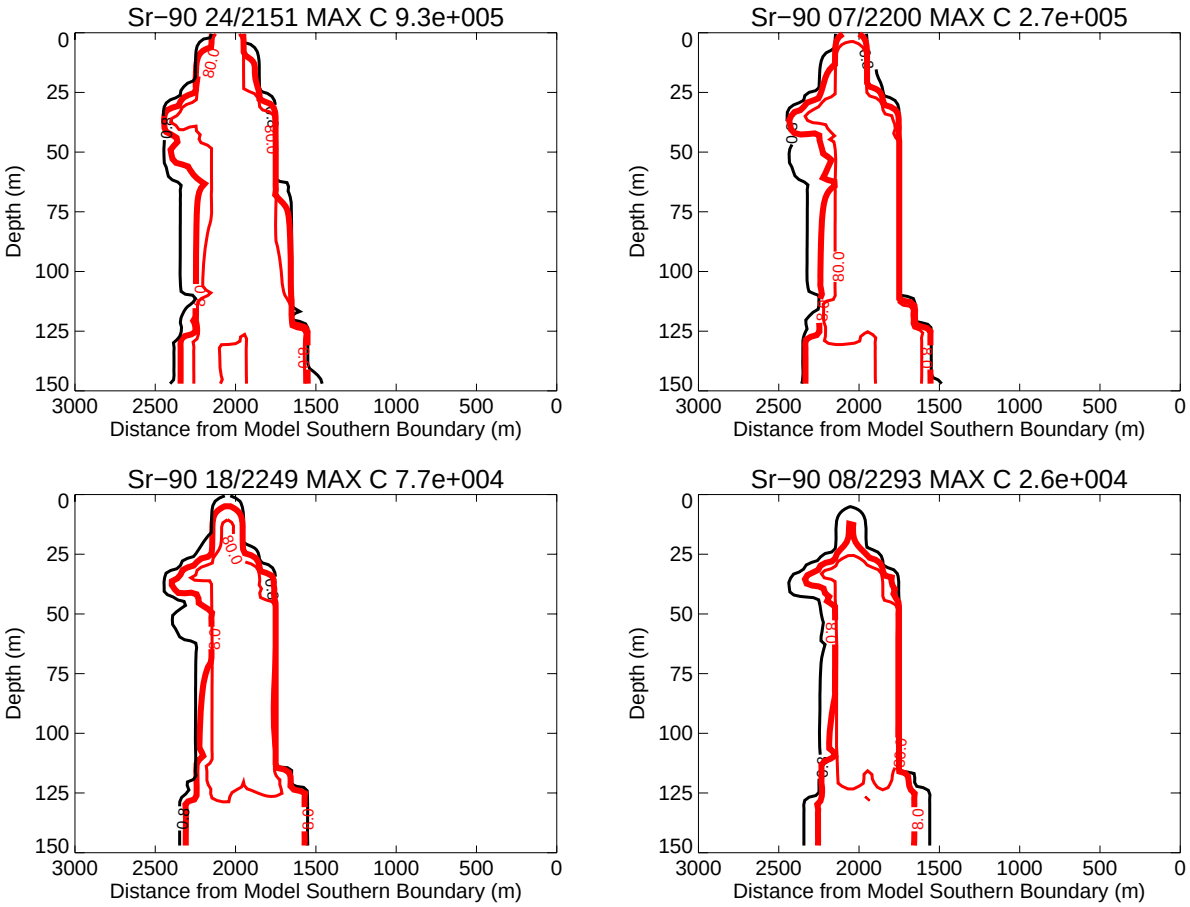

Figure J-9-13. Sr-90 vadose zone concentrations from CPP-79 deep (vertical contours) (pCi/L) (continued) (MCL = thick red line, 10*MCL = thin red line, MCL/10 = black line).

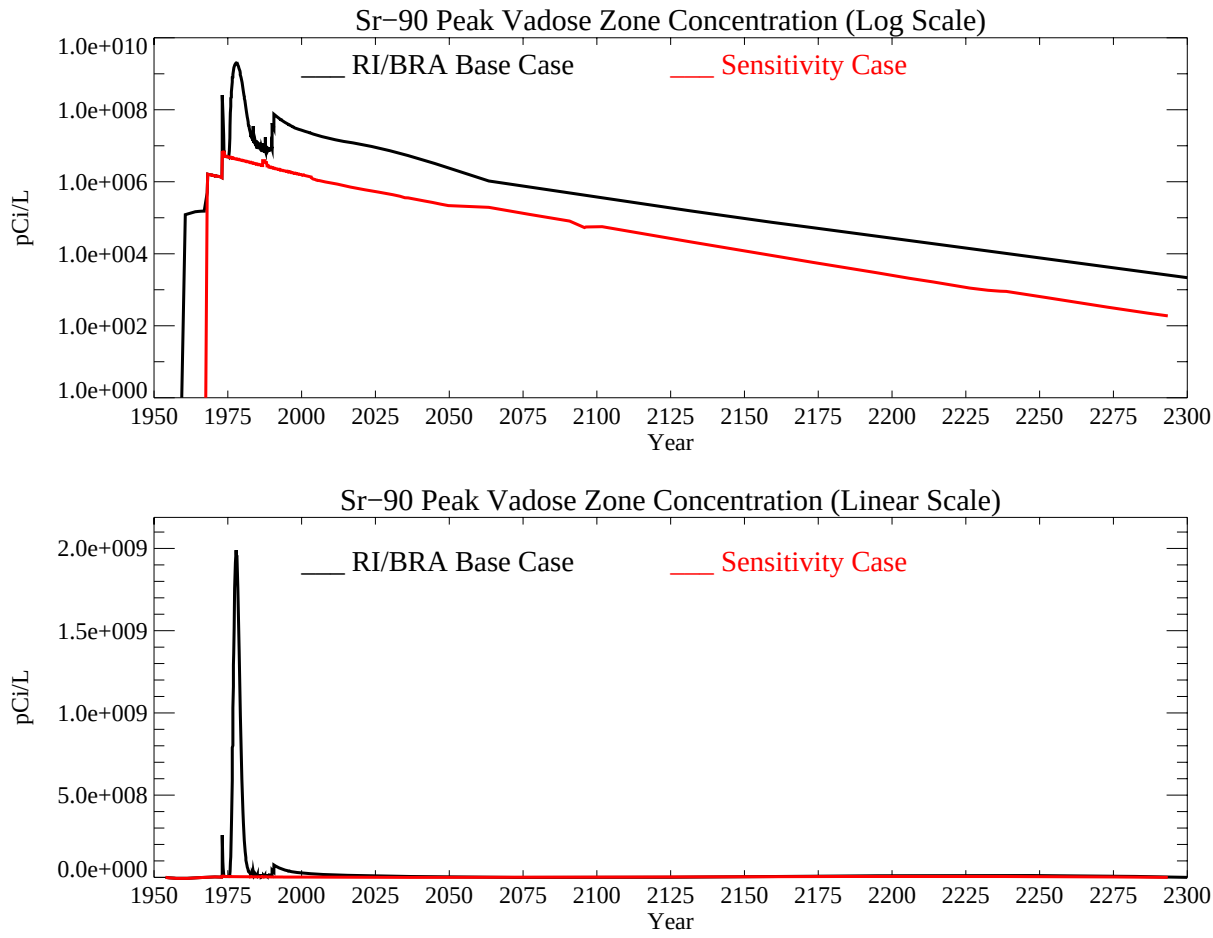

Figure J-9-14. Sr-90 peak vadose zone concentrations from CPP-79 deep (pCi/L) with the RI/BRA model in black and the CPP-79 deep source in red.

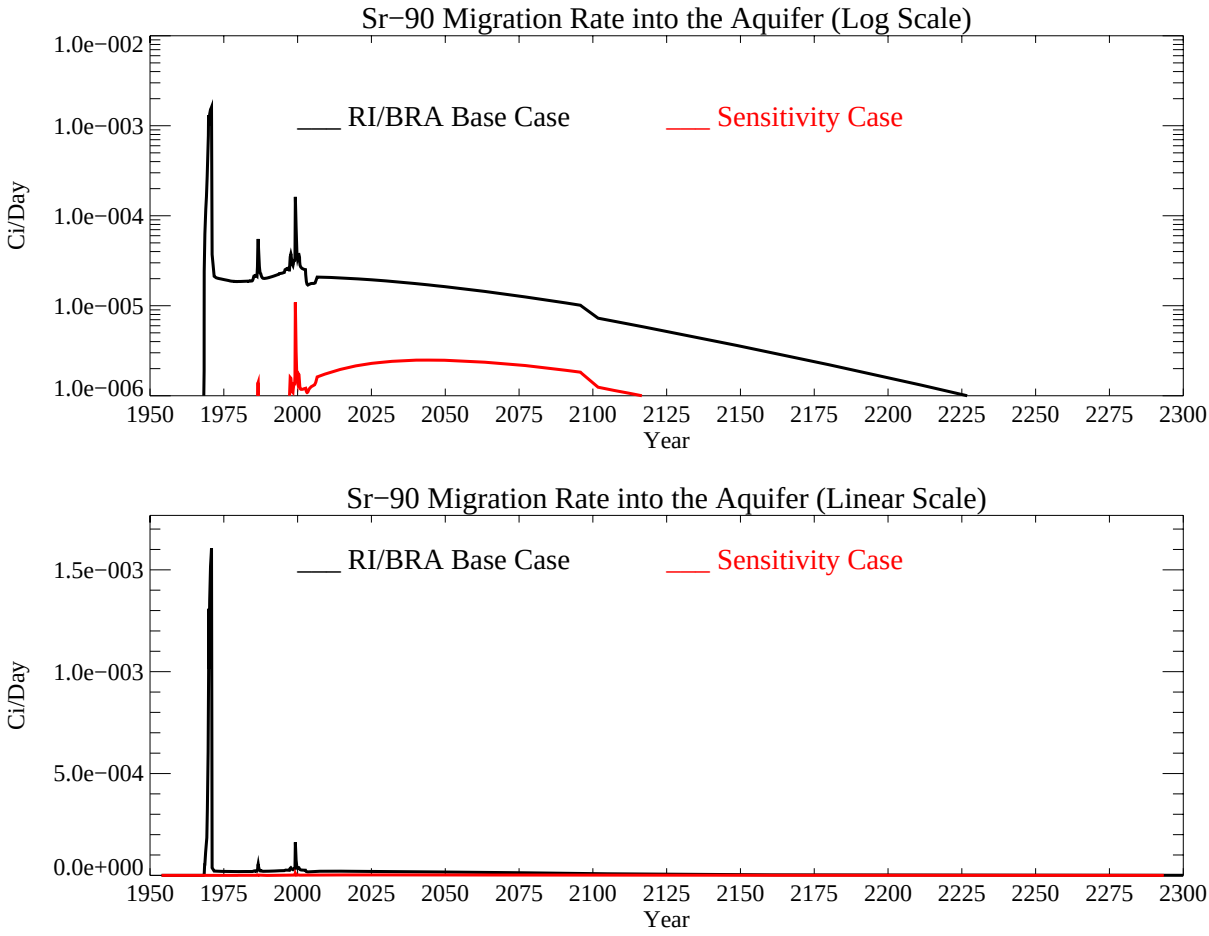

Figure J-9-15. Sr-90 activity flux into the aquifer from CPP-79 deep (Ci/day) with the RI/BRA model in black, and the CPP-79 deep source in red.

J-9.2.2 Aquifer Sr-90 Simulation Results

The distribution of Sr-90 in the aquifer for the time period spanning 1979-2096 is shown in the far-field in Figure J-9-16, and in the near-field in Figure J-9-17 for the 2096-2249 time period. The isopleths for year 2005 are provided to indicate that the aquifer is currently being impacted by Site CPP-79 deep. The area predicted to be impacted by CPP-79 deep is considerably smaller than that impacted by the injection well, the failure of the injection well, and other Sr-90 sources.

As shown in Figure J-9-18, the largest aquifer impact occurs in the 2000-time frame, with concentrations in the aquifer approaching 13 pCi/L. The predicted peak Sr-90 concentration in the year 2095 is 4.6 pCi/L, about equal to that of the contribution from non-tank farm sources, and about one quarter of the total aquifer impact in 2095. Although the concentrations from this source are not predicted to be less than the MCL by 2000, the area impacted by CPP-79 above the MCL by itself is small. It is the overlap of this area with that caused by CPP-31 that contributes to aquifer concentrations exceeding the MCL over a larger area.

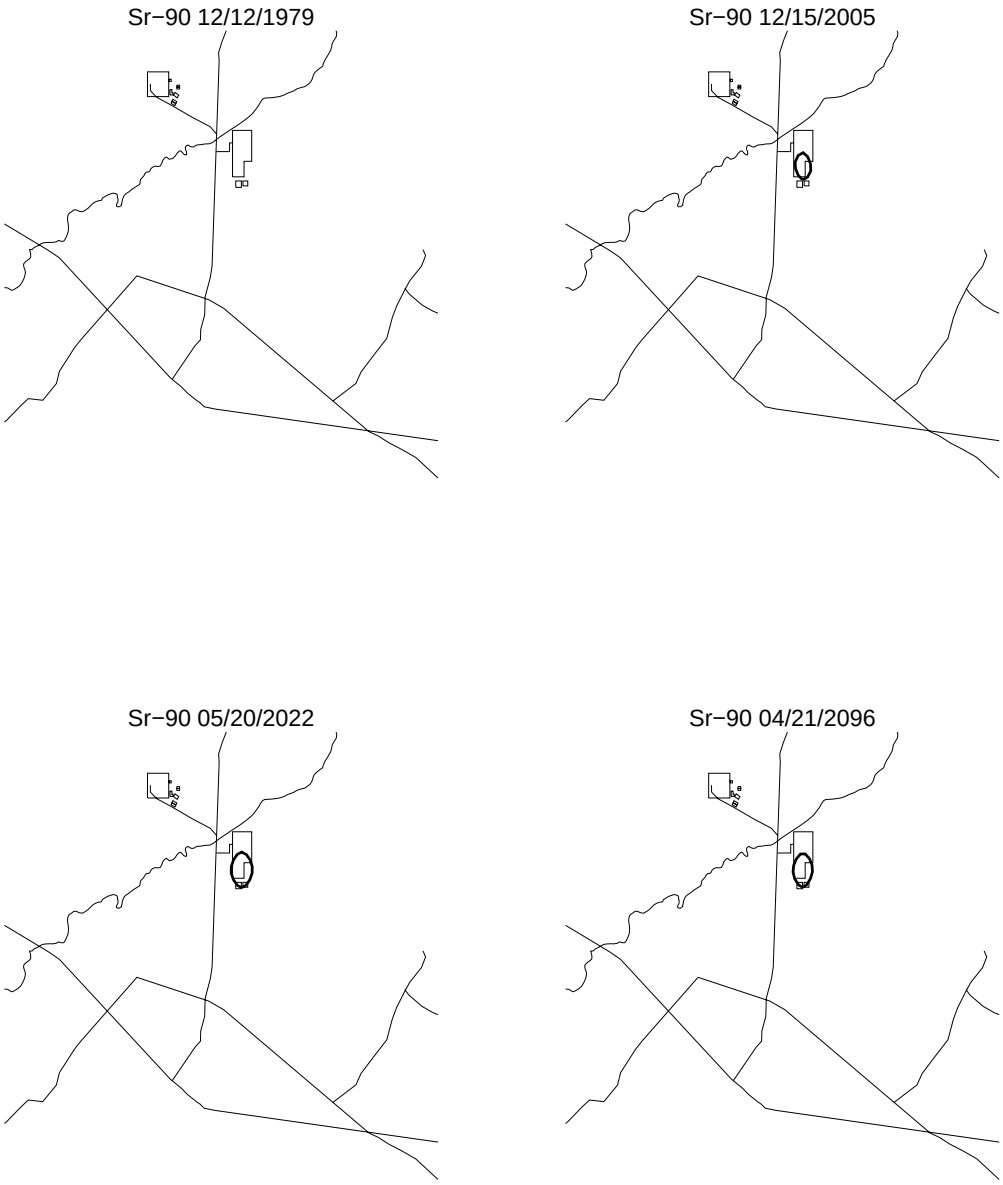

Figure J-9-16. Sr-90 aquifer concentration contours from CPP-79 deep (pCi/L) (MCL = thick red line, 10*MCL = thin red line, MCL/10 = black line).

Figure J-9-17. Sr-90 aquifer concentration contours from CPP-79 deep (pCi/L) (continued) (MCL = thick red line, 10*MCL = thin red line, MCL/10 = black line).

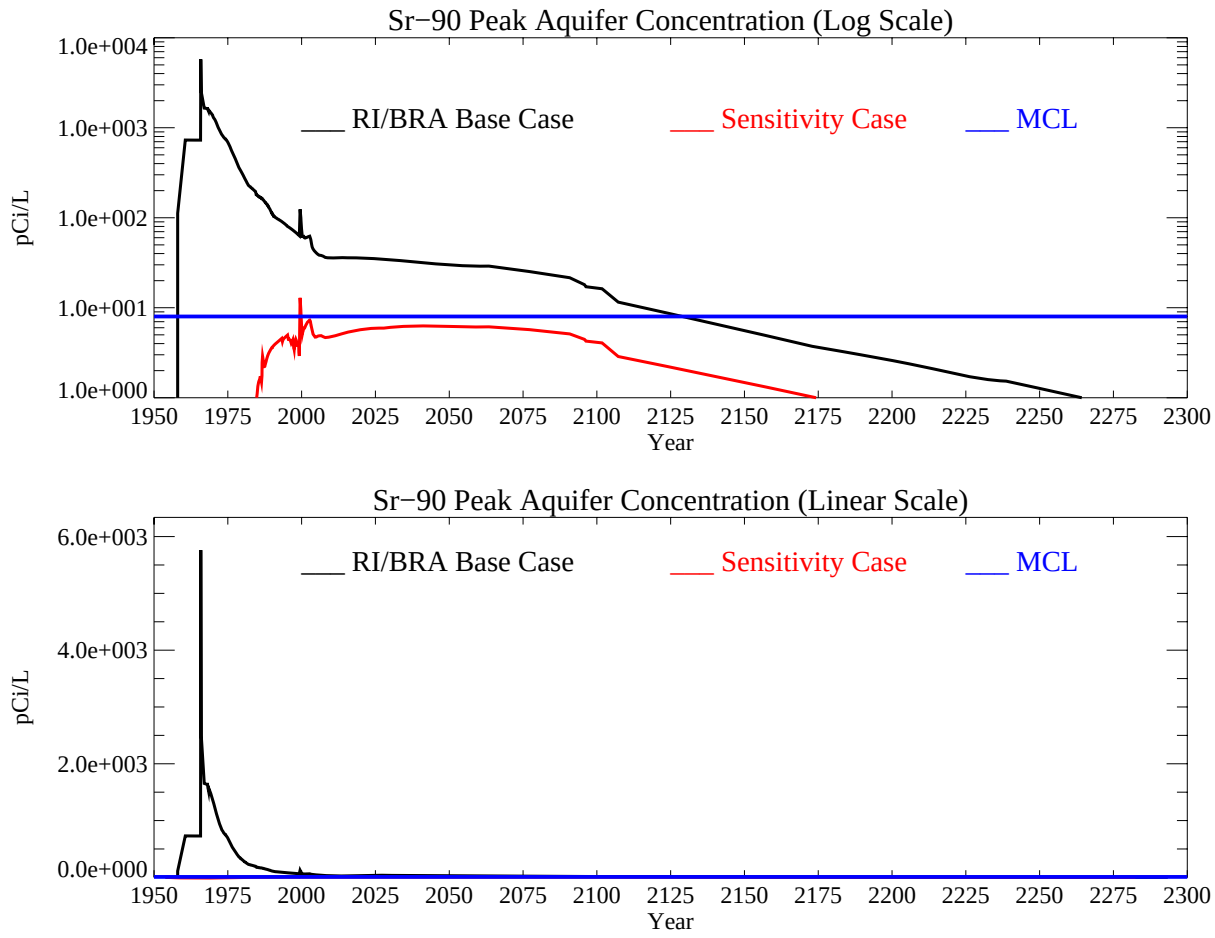

Figure J-9-18. Sr-90 peak aquifer concentrations from CPP-79 deep (pCi/L) with the MCL in blue, RI/BRA model in black and the CPP-79 deep source in red.